Original Article

Yonsei Med J 2018 Sep;59(7):887-896
https://doi.org/10.3349/ymj.2018.59.7.887

Yonsei Medical Journal
YMJ
pISSN: 0513-5796 · eISSN: 1976-2437

Diagnostic Ability of Swept-Source and Spectral-Domain Optical Coherence Tomography for Glaucoma

Sang Yeop Lee, Hyoung Won Bae, Gong Je Seong, and Chan Yun Kim

Department of Ophthalmology, Severance Hospital, Institute of Vision Research, Yonsei University College of Medicine, Seoul, Korea.

Purpose: To compare the diagnostic abilities of swept-source optical coherence tomography (OCT) [Deep Range Imaging OCT-1 (DRI-OCT)] and spectral-domain OCT (Cirrus HD-OCT) for glaucoma in Korean adults.

Materials and Methods: This retrospective study involved measuring peripapillary retinal nerve fiber layer (PP-RNFL) thickness, full macular thickness, and ganglion cell-inner plexiform layer (GC-IPL) thickness on two different OCT systems. We used three-dimensional optic disc scanning of DRI-OCT and included 12 clock-hour sectors for measurement of the PP-RNFL. Areas under receiver operating characteristic curves (AUCs) were calculated and compared to determine how well each system could distinguish control and glaucomatous patients.

Results: Ninety-one healthy and 58 glaucomatous eyes were included. Both systems could clearly distinguish between control eyes and eyes with moderate to severe glaucoma. Among all sectors, the AUC values of areas associated with glaucoma were >0.7 for both OCTs. The PP-RNFL sector of highest AUC value on both OCTs was the inferior sector of the clock-hour map (0.968 and 0.959 in DRI-OCT and Cirrus HD-OCT, respectively). Among macular thickness sectors, AUC values were highest on both OCTs for the outer inferior sector (0.859 and 0.853 in DRI-OCT and Cirrus HD-OCT, respectively). The GC-IPL also provided high diagnostic values (DRI-OCT and Cirrus HD-OCT were the best in the average and inferior sectors, respectively).

Conclusion: Although the two OCT systems provided different thickness measurements, DRI-OCT exhibited as good, if not better, diagnostic ability for glaucoma as Cirrus HD-OCT in Korean adults.

Key Words: Glaucoma, diagnostic ability, spectral domain optical coherence tomography, swept source optical coherence tomography

INTRODUCTION

Glaucoma is a disease that leads to blindness, and early diagnosis is important to maintain vision. Because glaucoma patients do not experience the subjective symptoms of glaucomatous visual field loss or visual damage until the disease has progressed to an advanced stage, the role of ophthalmic examinations for measurement of retinal nerve fiber layer (RNFL) thickness or visual field is important for ensuring timely diagnosis. Optical coherence tomography (OCT) is a well-known modality providing objective evaluation of structural alterations in the optic nerve head or macular area.[1-3] The development of OCT from time-domain OCT to spectral-domain OCT has increased the resolution and acquisition speed of OCT images, as well as the accuracy of glaucoma diagnosis.[4,5] Recently, swept-source OCT, a new OCT system with a novel light source and detector, has been introduced. This device uses a 1050-nm tunable light source with narrow line width and a simply designed light detector. The long-wave light source allows for the identification of the deep retinal structure. In addition, a large covering range (from the macula to the optic disc) can be obtained using the wide scanning mode, with a scanning speed up to 100000 A-scans/s. We previously compared swept-source OCT and spectral-domain OCT in terms of artifact type and frequency in source data and final

Received: March 22, 2018 **Revised:** June 25, 2018
Accepted: July 3, 2018
Corresponding author: Chan Yun Kim, MD, PhD, Department of Ophthalmology, Severance Hospital, Institute of Vision Research, Yonsei University College of Medicine, 50-1 Yonsei-ro, Seodaemun-gu, Seoul 03722, Korea.
Tel: 82-2-2228-3570, Fax: 82-2-312-0541, E-mail: kcyeye@yuhs.ac

•The authors have no financial conflicts of interest.

print out,[6] and measured repeatability and agreement between the two types of OCT.[7] From these studies, we verified that swept-source OCT provides results that are sufficiently reliable to be used in clinical practice. Determining the diagnostic ability of swept-source OCT for glaucoma was the next step, and several studies were conducted to compare the diagnostic ability between spectral-domain OCT and swept-source OCT.[8-11] However, most studies used Spectralis OCT (Heidelberg Engineering, Heidelberg, Germany) as spectral-domain OCT.[9-11] Only one study used Cirrus HD-OCT (Carl Zeiss Meditec, Inc., Dublin, CA, USA) with the wide angle mode of swept-source OCT to measure the thickness of macular or peripapillary area in a non-Asian population.[8]

Therefore, in the present study, we compared the diagnostic ability of swept-source OCT [Deep Range Imaging OCT-1 (DRI-OCT), software version 9.1.2.28693, Topcon, Tokyo, Japan] and spectral-domain OCT (Cirrus HD-OCT, software version 6.0.2.81) for glaucoma in the adult Korean population using wide-angle and three-dimensional (3D) optic disc protocols for DRI-OCT.

MATERIALS AND METHODS

This study was approved by the Institutional Review Board of Yonsei University Severance Hospital (Reference No. 4-2017-0112). All conducted research adhered to the tenets of the Declaration of Helsinki, and informed consent was obtained. All subjects were examined at the glaucoma clinic of the Department of Ophthalmology at Severance Hospital, Yonsei University School of Medicine in Seoul, Korea. We reviewed the medical records of 185 normal and primary open angle glaucoma (POAG) subjects for whom peripapillary retinal nerve fiber layer (PP-RNFL), ganglion cell-inner plexiform layer (GC-IPL), and macular thickness measurements were obtained using both DRI-OCT and Cirrus HD-OCT on the same day, between June and December 2014. All subjects underwent ophthalmic examinations to evaluate Snellen best-corrected visual acuity, refractive spherical equivalent, and intraocular pressure using Goldmann applanation tonometry. IOL Master (Carl Zeiss Meditec AG, Jena, Germany) and ultrasonic pachymetry (DGH-1000; DGH Technology, Inc., Frazer, PA, USA) were used to measure axial length and central corneal thickness, respectively. RNFL defect and optic disc evaluation were performed using a +90 diopter lens and a red-free photograph (VISUCAM 200; Carl Zeiss Meditec AG). To screen POAG, a visual field test (24-2 Swedish Interactive Threshold Algorithm, Humphrey Visual Field Analyzer; Carl Zeiss Meditec, Inc., Dublin, CA, USA) was conducted. All examination results were reviewed by two glaucoma specialists (S.Y.L. and H.W.B.) to recheck the diagnosis results of medical records. Another glaucoma specialist (C.Y.K.) confirmed medical records again, if there was a disagreement.

Subjects

A group of normal patients was included in the study to serve as a control group. All control subjects were at least 19 years of age and had a best-corrected visual acuity of 20/25 or better. Only individuals with a normal fundus, intraocular pressure < 21 mm Hg, and normal visual field were included in the control group. The inclusion criteria for control group in this study were the same as those in a previous study,[7] since the current study was conducted as a follow-up to the previous study. Subjects were excluded from participation if they had an spherical equivalent larger than ±5 diopter, a cylindrical refractive error larger than 3 diopter, an axial length longer than 26.5 mm, any type of cataract more severe than a Grade 3 (Lens Opacities Classification System III[12]), a pre-existing optic nerve or retinal abnormality, a systemic or ocular condition associated with visual field defects, previous intraocular surgery, or glaucomatous changes discovered during study assessments. Subjects showing an image quality score of DRI-OCT <60 or signal strength of Cirrus HD-OCT <6 were also excluded.

Subjects placed into POAG study groups had glaucomatous optic nerve head changes related to a visual field defect that satisfied at least two Anderson and Patella criteria with open angle structure. These patients had undergone at least three visual field tests, demonstrating a visual field defect in at least three tests. Glaucoma patients were classified as either early or moderate-to-severe according to the Hodapp-Parrish-Anderson criteria.[13] Inclusion criteria regarding age and vision and exclusion criteria regarding refractive error, cataract status, medical history, and OCT quality score were identical to those used for the control group. In addition, other types of glaucoma were also excluded. For glaucomatous subjects, the eye with a more severe glaucoma status was chosen as the study eye. If subjects had a similar glaucoma severity in both eyes, the study eye was randomly selected. For subjects with normal eyes, the study eye was also randomly selected.

Thickness measurements using optical coherence tomography

For Cirrus HD-OCT scans, the optic disc cube 200×200 and macular cube scan 512 A-scans×128 B-scans protocols were used to measure PP-RNFL, macular, and GC-IPL thickness. To measure PP-RNFL thickness from Cirrus HD-OCT scans, a scan circle of 3.46 mm in diameter was used. The 3D optic disc and wide scan protocols were used to measure PP-RNFL, macular, and GC-IPL thickness using DRI-OCT. The 3D optic disc scan is comprised of 512 A-scans×256 B-scans covering a 6×6 mm square area centered on the optic disc. Data along a scan circle of 3.4 mm in diameter was used to evaluate PP-RNFL thickness. The 3D wide scan images a 12×9 mm rectangular area centered between the optic disc and the fovea. The final scan is composed of 512 A-scans×256 B-scans. This wide scan was used to evaluate macular and GC-IPL thickness.

A total of 17, 10, and seven retinal sectors were investigated

https://doi.org/10.3349/ymj.2018.59.7.887

for PP-RNFL, macular, and GC-IPL evaluations, respectively. All thickness data were obtained using the automated segmentation algorithms of each OCT device. The PP-RNFL measurements were obtained by measurements in four and 12 sectors (Fig. 1A and B, respectively). To classify measurement areas, quadrant PP-RNFL sector names were started with the number 4 and 12 clock hour sector names were started with the number 12. The macular thickness was obtained in each of the nine Early Treatment Diabetic Retinopathy Study (Fig. 1C) sectors. The diameters of three concentric circles that make up the Early Treatment Diabetic Retinopathy Study sector grid were 1, 3, and 6 mm. The GC-IPL was measured in each of six sectors (Fig. 1D). With these sectorial thicknesses, the average thickness of the total measurement area was also obtained for PP-RNFL (PP Aver), macular (Macular Aver), and GC-IPL (GC-IPL Aver) evaluations.

Statistical analyses

All statistical analyses were performed using SAS statistical software (version 9.2; SAS Inc., Cary, NC, USA). Data were compared between study groups using analysis of variance and chi-squared tests. The predictive power for glaucoma was compared between the two OCT systems using the receiver operating characteristic (ROC) curve. Areas under ROC curves (AUCs) were calculated and compared among control, early glaucoma, and moderate-to-severe glaucoma groups using the Delong method.[14] Statistical significance was defined as $p<0.05$.

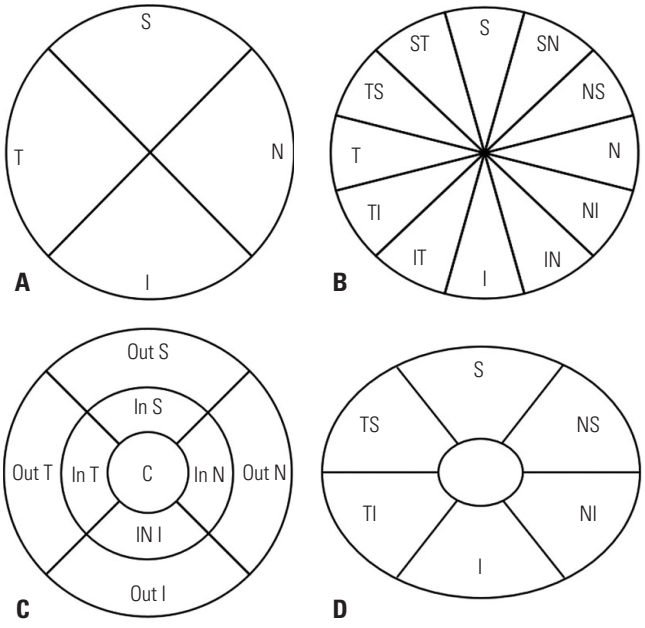

Fig. 1. Sectors used for optical coherence tomography (OCT) thickness measurements of peripapillary retinal nerve fiber layer thickness in both OCT systems (A: 4 sectors, B: 12 sectors). Sectors used for macular thickness (C) and ganglion cell inner plexiform layer thickness (D) measurements are also shown. All sectors shown are those used for right eye analyses. S, superior; N, nasal; I, inferior; T, temporal; SN, superonasal; NS, nasosuperior; NI, nasoinferior; IN, inferonasal; IT, inferotemporal; TI, temporoinferior; TS, temporosuperior; ST, superotemporal; Out S, outer superior; Out N, outer nasal; Out I, outer inferior; Out T, outer temporal; In S, inner superior; In N, inner nasal; In I, inner inferior; In T, inner temporal.

RESULTS

Among 185 subjects, 36 subjects were excluded. Among the excluded subjects, 18 subjects had a false diagnosis, and 11 subjects showed low OCT image quality. Finally, 91 eyes of 91 subjects were normal and 58 eyes of 58 subjects were glaucomatous. Of the 58 glaucomatous eyes, 32 had early disease and 26 had moderate-to-severe disease. Table 1 summarizes the subject characteristics. None of the study groups showed significant differences in any systemic or ocular characteristic, with the exception of the visual field mean deviation.

Thickness comparison among control and study groups in each OCT system

All measurement sectors showed significant thickness differences among control, early glaucoma, and moderate-to-severe glaucoma patients, except for four sectors in DRI-OCT measurements and nine sectors in Cirrus HD-OCT measurements (Table 2). The sectors that did not show any significant differences were areas of low importance in the diagnosis of glaucoma. Additionally, each retinal layer was thickest in control eyes and thinnest in the moderate-to-severe glaucoma eyes in every sector examined, even in sectors where there were no significant differences.

Comparison of glaucoma discrimination ability

To determine how effectively each OCT system discriminated between normal and glaucomatous eyes, AUC values were examined in each sector (Table 3, Figs. 2, 3, and 4; only the ROC

Table 1. Subjects and Ocular Characteristics

	Control (n=91)	Glaucoma (n=58)		
		Early (n=32)	Moderate to severe (n=26)	*p* value*
Age (yr)	54.3±15.81	54.6±14.72	54.4±12.33	0.832
Sex (M:F)	1:1.4	1:1.3	1:1.4	0.913
CCT (mm)	540.2±33.22	532.7±31.0	536.8±32.3	0.543
IOP (mm Hg)	14.3±2.63	14.2±2.35	13.6±2.48	0.274
AXL (mm)	23.5±1.40	23.7±1.40	23.4±1.57	0.262
>25.0 to ≤26.5	4 (4.4)	2 (6.3)	2 (8.3)	
>23.0 to ≤25.0	87 (95.6)	30 (93.8)	24 (92.3)	
SE (D)	-1.31±2.31	-1.32±3.04	-1.18±2.94	0.681
MD (dB)	-0.65±1.53	-2.38±1.55	-11.90±6.20	<0.001

CCT, central corneal thickness; IOP, intraocular pressure; AXL, axial length; SE, spherical equivalent; MD, mean deviation of visual field testing; SD, standard deviation.
Data are presented as mean±SD or number (%).
*ANOVA or chi-square test was used for statistical analyses.

curves for sectors of PP Aver, Macular Aver, and GC-IPL Aver are presented). In most sectors, the highest AUC value was obtained with both OCT data when the control and moderate-to-severe glaucoma groups were compared. PP-RNFL measurements revealed three sectors (4 nasal, 12 superior, and 12 nasosuperior) that had significantly different AUC values between the two OCT systems for control versus early glaucoma comparisons (Table 3, p=0.017, p=0.048, and p=0.005, respectively). Among these sectors, 12 superior sectors showed AUC values >0.7 in both OCT devices. Six different sectors (4 nasal, 12 superior, 12 superonasal, 12 nasosuperior, 12 nasal, and 12 nasoinferior) had significantly different PP-RNFL AUC values

Table 2. Average Retinal Layer Thickness in Normal and Glaucomatous Eyes

	DRI-OCT (Mean±SD)				Cirrus HD OCT (Mean±SD)			
	Control (n=91)	E (n=32)	MS (n=26)	Overall *p* value*	Control (n=91)	E (n=32)	MS (n=26)	Overall *p* value*
PP-RNFL								
PP Aver	107.31±10.67	87.12±16.61	67.96±14.97	<0.001	94.23±8.96	79.91±12.56	66.96±11.81	<0.001
4T	81.21±14.33	72.08±13.52	63.82±14.25	<0.001	71.44±13.45	63.22±12.41	57.31±12.66	<0.001
4S	132.72±17.50	107.96±24.16	84.34±25.77	<0.001	116.98±15.76	96.78±21.46	80.62±21.04	<0.001
4N	74.9±16.11	65.77±17.60	55.723±15.78	<0.001	65.96±10.35	64.25±10.27	61.69±8.94	0.158
4I	140.57±18.47	107.53±29.10	69.19±23.86	<0.001	121.47±20.42	95.44±22.76	68.58±19.75	<0.001
12T	67.6±11.21	65.01±12.68	62.88±10.55	0.146	55.99±10.59	53.75±11.15	52.04±9.22	0.197
12TS	95.9±19.37	89.27±23.07	71.17±22.06	<0.001	84.58±16.68	76.47±18.73	63.89±15.8	<0.001
12ST	142.38±23.57	118.33±29.21	80.14±32.65	<0.001	130.22±21.29	106.81±24.69	78.42±24.99	<0.001
12S	136.44±27.28	105.22±30.49	88.49±23.56	<0.001	119.56±25.51	98.28±30.19	84.96±23.88	<0.001
12SN	118.83±27.01	97.99±29.94	83.74±29.49	<0.001	101.75±23.55	83.94±23.39	80.77±19.95	<0.001
12NS	87.25±21.63	79.48±29.13	61.43±24.07	<0.001	76.67±16.18	75±14.27	68.73±12.22	0.066
12N	63.44±13.42	61.27±22.17	50.34±15.96	<0.001	57.98±10.02	56.845±9.64	55.96±10.99	0.780
12NI	73.79±19.19	65.47±18.10	56.49±15.63	<0.001	62.26±11.22	60.6±13.69	60.01±10.43	0.385
12IN	115.7±23.48	95.71±28.66	74.76±21.61	<0.001	96.69±18.55	82.22±19.86	67.58±13.51	<0.001
12I	155.5±29.31	114.91±32.39	73.07±30.96	<0.001	132.01±26.05	101.09±28.45	68.12±22.55	<0.001
12IT	150.41±27.23	107.29±38.38	61.34±37.68	<0.001	139.6±23.51	98.84±35.41	66.89±30.48	<0.001
12TI	80.4±18.04	71.48±25.90	58.69±17.32	<0.001	73.71±19.06	60.16±12.06	54.81±17.66	<0.001
MT								
MT Aver	270.54±13.92	260.47±16.51	253.24±16.89	<0.001	279.09±13.27	269.38±16.9	260.58±17.54	<0.001
Center	225.60±18.37	224.77±15.60	223.33±25.51	0.484	245.63±19.45	245.37±13.92	241.58±27.18	0.387
In T	289.06±16.29	278.34±13.28	273.90±20.28	<0.001	309.84±18.80	303.31±16.19	302.81±20.56	0.026
In S	299.15±16.48	292.93±13.44	291.83±23.66	0.072	319.01±18.14	314.34±15.83	312.46±22.22	0.195
In N	299.07±17.73	295.43±15.15	295.28±20.03	0.517	316.67±18.84	315.3±17.53	313.54±28.21	0.753
In I	297.83±17.40	287.87±17.20	281.37±25.27	<0.001	314.95±18.07	304.81±19.16	297±27.38	<0.001
Out T	253.67±14.58	241.4±16.01	234.86±18.76	<0.001	270.48±21.67	257.31±20.86	255.73±24.15	<0.001
Out S	268.39±15.03	259.55±21.02	249.03±18.75	<0.001	280.01±15.01	273±21.33	260.77±18.31	<0.001
Out N	281.26±15.95	271.36±19.33	268.87±20.36	<0.001	287.55±22.30	284.56±23.22	275.12±26.60	0.060
Out I	255.20±14.52	239.5±21.88	226.58±28.91	<0.001	265.8±13.95	251.16±23.1	237.54±27.38	<0.001
GC-IPL								
GC-IPL Aver	70.57±5.72	64.64±6.90	61.44±7.82	<0.001	81.3±7.02	73.94±8.57	67.54±10.38	<0.001
TS	72.72±5.85	67.47±6.67	63.47±8.05	<0.001	80.65±6.60	73.59±8.64	66.69±11.53	<0.001
S	69.03±5.91	63.87±7.63	59.33±10.04	<0.001	82.31±7.23	77.19±10.07	70.46±13.30	<0.001
NS	72.91±6.73	69.46±7.14	67.61±9.13	<0.001	83.54±7.74	79.41±8.71	77.62±10.69	<0.001
NI	70.96±6.22	64.81±8.26	62.80±8.19	<0.001	80.98±7.53	75.47±10.05	70.62±10.28	<0.001
I	65.53±5.96	57.83±8.58	56.31±10.79	<0.001	79.31±7.46	70.03±11.23	60.54±14.23	<0.001
TI	72.19±6.35	64.42±8.58	60.69±10.23	<0.001	81.21±7.95	69.88±13.16	59.27±15.01	<0.001

SD, standard deviation; E, early glaucoma; MS, moderate to severe glaucoma; PP-RNFL, peripapillary retinal nerve fiber layer thickness; PP Aver, average PP-RNFL; MT, macular thickness; MT Aver, average MT; GC-IPL, ganglion cell-inner plexiform layer thickness; GC-IPL Aver, average GC-IPL; S, superior; N, nasal; I, inferior; T, temporal; SN, superonasal; NS, nasosuperior; N, nasoinferior; IN, inferonasal; IT, inferotemporal; TI, temporoinferior; TS, temporosuperior; ST, superotemporal; Out S, outer superior; Out N; outer nasal; Out I, outer inferior; Out T, outer temporal; In S, inner superior; In N, inner nasal; In I, inner inferior; In T, inner temporal; TS, temporosuperior; NI, nasoinferior.
*ANOVA test was used for statistical analyses.

https://doi.org/10.3349/ymj.2018.59.7.887

when the control and moderate-to-severe glaucoma groups were compared (Table 3, p=0.003, 0.013, 0.022, 0.003, 0.021, and 0.001, respectively). Among these sectors, 12 superior, 12 superonasal, and 12 inferonasal sectors showed AUC values >0.7 in both OCT devices. Only 12 superonasal sectors had a significantly different AUC value between OCT modalities in early glaucoma versus moderate to severe glaucoma comparisons (Table 4). Most sectors showing significantly different AUC values were nasal areas of low importance for glaucoma diagnosis. The measurement sectors indicating superotempo-

Table 3. Receiver Operating Characteristic Curve Comparison for Glaucoma Discrimination Ability between Control Group and Glaucoma Group

	Control vs. Early glaucoma (C-E)					Control vs. Moderate to severe glaucoma (C-MS)				
	DRI		Cirrus		p value*	DRI		Cirrus		p value*
	AUC	95% CI	AUC	95% CI		AUC	95% CI	AUC	95% CI	
PP-RNFL										
PP Aver	0.851	0.755–0.947	0.818	0.715–0.921	0.242	0.979	0.956–1.000	0.951	0.906–0.996	0.070
4T	0.689	0.579–0.800	0.691	0.582–0.799	0.951	0.811	0.711–0.912	0.789	0.678–0.899	0.314
4S	0.824	0.727–0.919	0.780	0.673–0.885	0.140	0.932	0.874–0.991	0.899	0.817–0.983	0.147
4N	0.649	0.537–0.761	0.554	0.437–0.671	0.017	0.795	0.708–0.882	0.627	0.510–0.744	0.003
4I	0.816	0.717–0.915	0.809	0.712–0.905	0.654	0.981	0.959–1.000	0.958	0.923–0.993	0.133
12T	0.599	0.483–0.714	0.575	0.464–0.687	0.468	0.614	0.494–0.735	0.601	0.482–0.720	0.673
12TS	0.618	0.495–0.740	0.638	0.519–0.756	0.59	0.795	0.687–0.903	0.827	0.727–0.927	0.275
12ST	0.745	0.642–0.848	0.773	0.680–0.866	0.364	0.938	0.890–0.987	0.943	0.901–0.985	0.779
12S	0.795	0.701–0.890	0.725	0.611–0.839	0.048	0.910	0.848–0.971	0.856	0.763–0.950	0.013
12SN	0.749	0.646–0.851	0.735	0.629–0.842	0.592	0.814	0.720–0.909	0.753	0.647–0.859	0.022
12NS	0.621	0.499–0.742	0.519	0.407–0.632	0.005	0.791	0.695–0.887	0.637	0.523–0.750	0.003
12N	0.578	0.457–0.699	0.525	0.410–0.641	0.616	0.720	0.610–0.830	0.546	0.412–0.680	0.021
12NI	0.638	0.523–0.753	0.562	0.439–0.686	0.061	0.746	0.642–0.851	0.539	0.419–0.660	0.001
12IN	0.712	0.595–0.829	0.695	0.582–0.809	0.564	0.904	0.836–0.972	0.899	0.838–0.960	0.793
12I	0.828	0.743–0.913	0.794	0.697–0.891	0.263	0.968	0.938–0.997	0.959	0.924–0.992	0.504
12IT	0.822	0.738–0.906	0.838	0.757–0.919	0.465	0.933	0.863–1.000	0.937	0.878–0.995	0.653
12TI	0.686	0.581–0.790	0.719	0.625–0.814	0.275	0.810	0.713–0.915	0.799	0.685–0.912	0.530
MT										
MT Aver	0.712	0.599–0.826	0.725	0.609–0.842	0.554	0.807	0.702–0.912	0.808	0.696–0.921	0.954
Center	0.500	0.384–0.617	0.558	0.447–0.668	0.605	0.575	0.454–0.696	0.582	0.458–0.705	0.811
In T	0.722	0.625–0.820	0.665	0.561–0.770	0.148	0.740	0.617–0.863	0.623	0.495–0.752	0.015
In S	0.637	0.531–0.742	0.571	0.457–0.686	0.060	0.592	0.452–0.732	0.573	0.435–0.711	0.494
In N	0.590	0.476–0.700	0.511	0.395–0.627	0.473	0.515	0.378–0.651	0.513	0.371–0.656	0.992
In I	0.675	0.564–0.784	0.661	0.549–0.773	0.554	0.713	0.579–0.846	0.724	0.589–0.859	0.548
Out T	0.761	0.660–0.862	0.716	0.602–0.829	0.282	0.808	0.683–0.933	0.713	0.584–0.842	0.043
Out S	0.690	0.574–0.805	0.668	0.549–0.788	0.262	0.795	0.691–0.899	0.782	0.678–0.886	0.496
Out N	0.670	0.549–0.792	0.553	0.434–0.672	0.006	0.681	0.554–0.808	0.635	0.506–0.763	0.338
Out I	0.772	0.664–0.881	0.754	0.637–0.870	0.431	0.859	0.746–0.973	0.853	0.737–0.969	0.473
GC-IPL										
GC-IPL Aver	0.747	0.644–0.849	0.751	0.649–0.853	0.788	0.832	0.726–0.938	0.862	0.759–0.965	0.053
TS	0.726	0.627–0.824	0.747	0.649–0.846	0.266	0.827	0.729–0.925	0.848	0.746–0.949	0.239
S	0.712	0.604–0.819	0.681	0.567–0.795	0.150	0.793	0.683–0.903	0.772	0.657–0.888	0.228
NS	0.642	0.528–0.755	0.655	0.543–0.768	0.342	0.680	0.561–0.800	0.671	0.553–0.787	0.587
NI	0.715	0.606–0.823	0.668	0.553–0.785	0.017	0.793	0.693–0.893	0.802	0.703–0.901	0.674
I	0.759	0.648–0.871	0.745	0.633–0.858	0.426	0.794	0.676–0.913	0.867	0.757–0.977	0.002
TI	0.758	0.653–0.862	0.762	0.652–0.872	0.780	0.820	0.700–0.940	0.853	0.739–0.966	0.062

AUC, area of under the receiver operating characteristic curve; PP-RNFL, peripapillary retinal nerve fiber layer thickness; PP Aver, average PP-RNFL; MT, macular thickness; MT Aver, average MT; GC-IPL, ganglion cell-inner plexiform layer thickness; GC-IPL Aver, average GC-IPL; S, superior; N, nasal; I, inferior; T, temporal; SN, superonasal; NS, nasosuperior; N, nasoinferior; IN, inferonasal; IT, inferotemporal; TI, temporoinferior; TS, temporosuperior; ST, superotemporal; Out S, outer superior; Out N, outer nasal; Out I, outer inferior; Out T, outer temporal; In S, inner superior; In N, inner nasal; In I, inner inferior; In T, inner temporal; TS, temporosuperior; NI, nasoinferior.
*Delong method was used for statistical analyses.

ral and inferotemporal directions, which were important area for glaucoma diagnosis, showed AUC values >0.7 or >0.8 in both OCT devices.

AUC values for macular thickness differed significantly between OCT systems in four sectors (Tables 3 and 4). These included the outer nasal sector in the control versus early glaucoma comparison (p=0.006), the inner temporal sector and outer temporal sectors in the control versus moderate to severe glaucoma comparison (p=0.015 and p=0.043, respectively), and the outer temporal sector in the early glaucoma versus

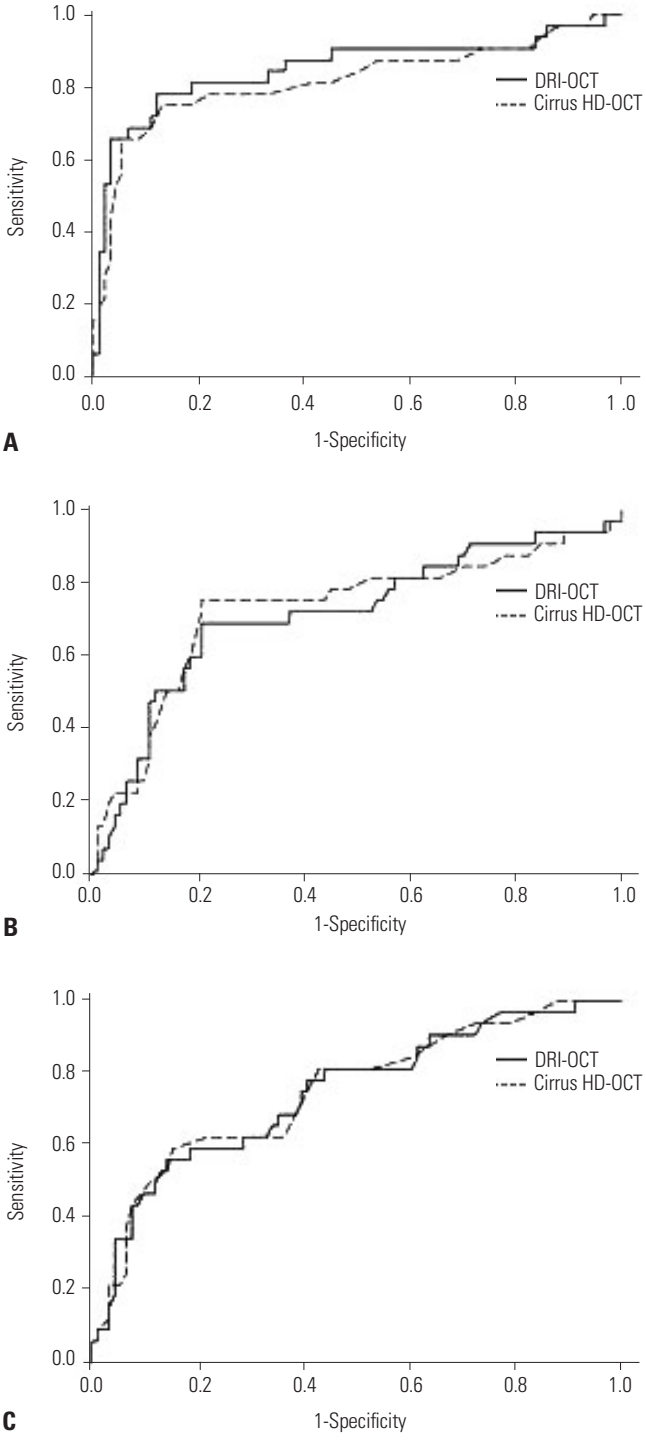

Fig. 2. Receiver operating characteristics curve of average peripapillary retinal nerve fiber layer thickness (A), macular thickness (B), and ganglion cell-inner plexiform layer thickness (C) measurements made with two optical coherence tomography (OCT) modalities (DRI-OCT and Cirrus HD-OCT) between control and early glaucoma.

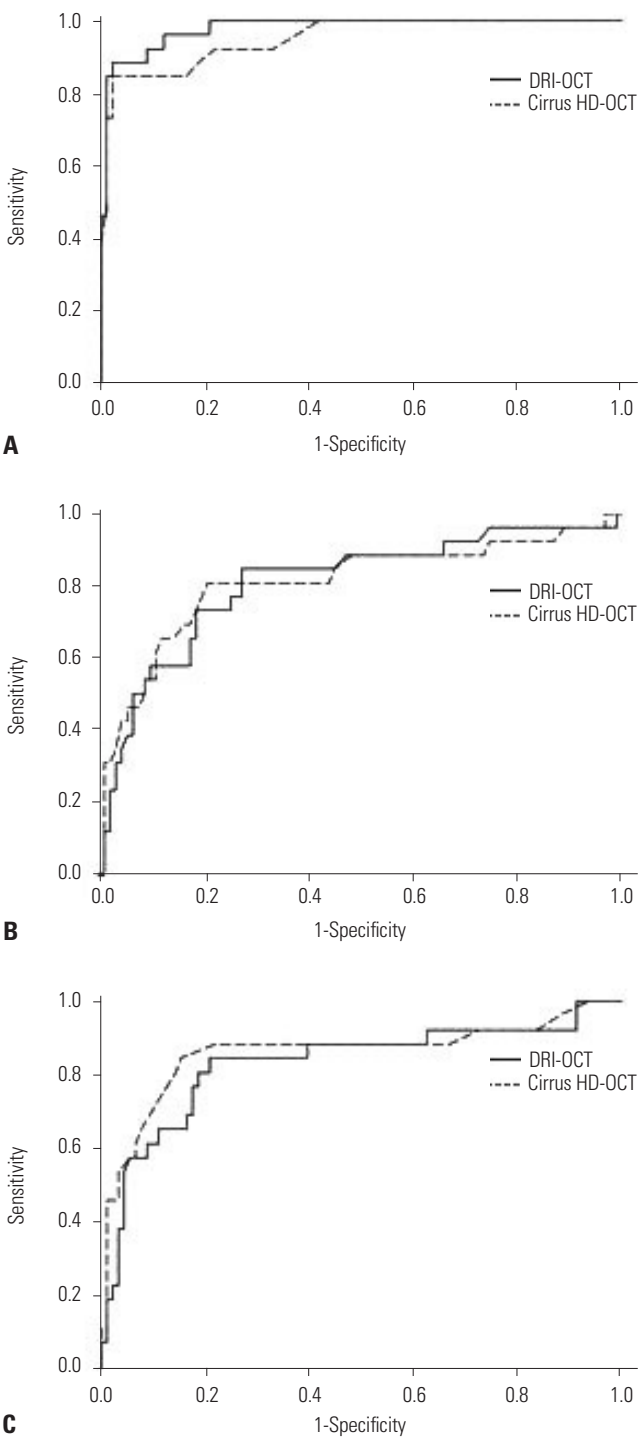

Fig. 3. Receiver operating characteristics curve of average peripapillary retinal nerve fiber layer thickness (A), macular thickness (B), and ganglion cell-inner plexiform layer thickness (C) measurements made with two optical coherence tomography (OCT) modalities (DRI-OCT and Cirrus HD-OCT) between control and moderate to severe glaucoma.

https://doi.org/10.3349/ymj.2018.59.7.887

moderate to severe glaucoma comparison (p=0.034) showing higher AUC in DRI-OCT than Cirrus HD-OCT.

Sector GC-IPL AUC measurements revealed four sectors with statistically significant differences between OCT modalities (Tables 3 and 4). The DRI-OCT AUC was significantly higher than the Cirrus HD-OCT AUC in the nasoinferior sector for the control versus early glaucoma comparison (p=0.017). However, the Cirrus HD-OCT AUC was significantly higher than

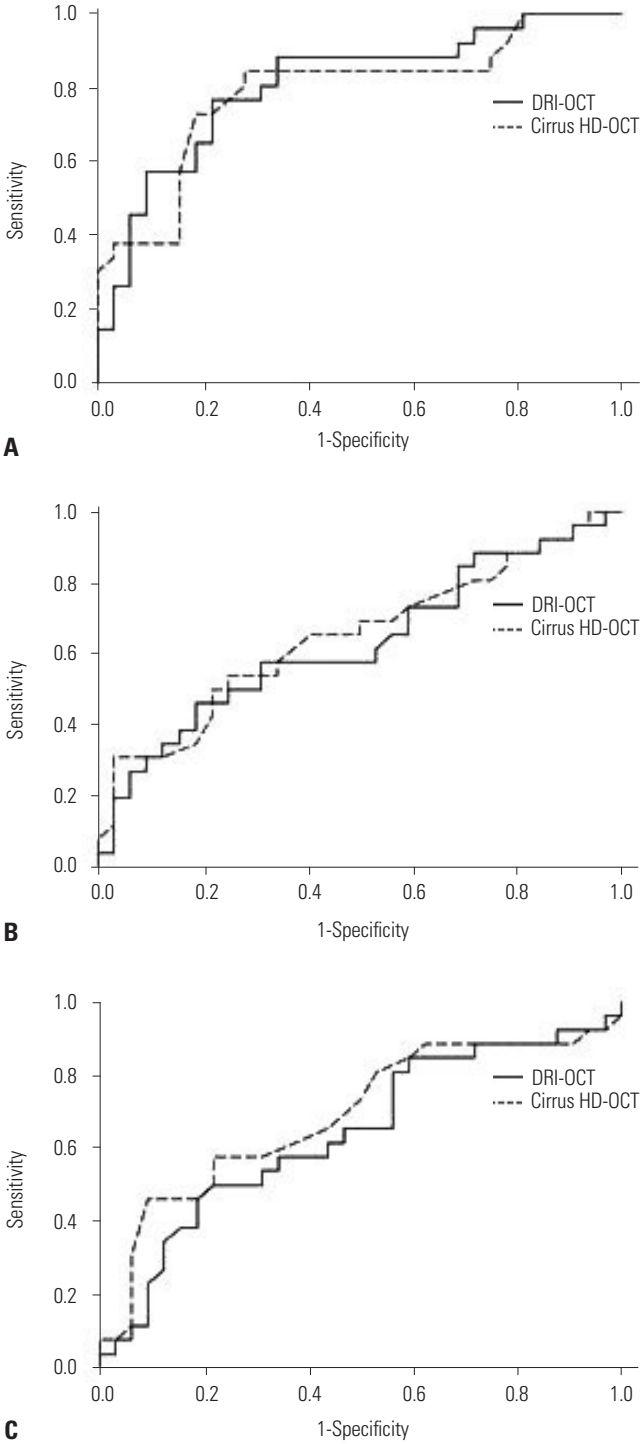

Fig. 4. Receiver operating characteristics curve of average peripapillary retinal nerve fiber layer thickness (A), macular thickness (B), and ganglion cell-inner plexiform layer thickness (C) measurements made with two optical coherence tomography (OCT) modalities (DRI-OCT and Cirrus HD-OCT) between early and moderate to severe glaucoma.

Table 4. Receiver Operating Characteristic Curve Comparison for Glaucoma Discrimination Ability between Early and Moderate to Severe Glaucoma

	Early vs. moderate to severe glaucoma (E-MS)				
	DRI		Cirrus		*p* value*
	AUC	95% CI	AUC	95% CI	
PP-RNFL					
PP Aver	0.810	0.696–0.925	0.792	0.669–0.915	0.634
4T	0.661	0.517–0.806	0.650	0.502–0.799	0.760
4S	0.748	0.614–0.881	0.721	0.584–0.858	0.351
4N	0.650	0.508–0.793	0.563	0.412–0.714	0.221
4I	0.862	0.764–0.960	0.831	0.722–0.939	0.269
12T	0.509	0.355–0.663	0.525	0.372–0.677	0.728
12TS	0.701	0.563–0.838	0.695	0.557–0.834	0.863
12ST	0.791	0.672–0.910	0.787	0.666–0.907	0.901
12S	0.668	0.523–0.809	0.646	0.501–0.791	0.584
12SN	0.622	0.473–0.773	0.503	0.349–0.657	0.005
12NS	0.666	0.526–0.806	0.621	0.475–0.770	0.357
12N	0.610	0.467–0.761	0.576	0.422–0.729	0.676
12NI	0.630	0.478–0.770	0.519	0.367–0.671	0.440
12IN	0.715	0.582–0.849	0.723	0.593–0.853	0.843
12I	0.826	0.718–0.930	0.823	0.716–0.929	0.920
12IT	0.814	0.691–0.937	0.770	0.639–0.901	0.195
12TI	0.688	0.546–0.831	0.686	0.537–0.834	0.939
MT					
MT Aver	0.629	0.480–0.780	0.648	0.502–0.795	0.509
Center	0.569	0.418–0.719	0.527	0.373–0.681	0.362
In T	0.606	0.446–0.766	0.508	0.350–0.665	0.510
In S	0.498	0.337–0.658	0.516	0.357–0.675	0.511
In N	0.579	0.422–0.734	0.513	0.355–0.672	0.660
In I	0.603	0.448–0.750	0.626	0.470–0.782	0.349
Out T	0.676	0.527–0.824	0.556	0.400–0.712	0.034
Out S	0.633	0.486–0.781	0.654	0.507–0.801	0.417
Out N	0.525	0.371–0.679	0.578	0.424–0.732	0.318
Out I	0.696	0.553–0.837	0.696	0.552–0.839	1.000
GC-IPL					
GC-IPL Aver	0.637	0.489–0.785	0.688	0.544–0.832	0.071
TS	0.663	0.516–0.810	0.693	0.549–0.837	0.294
S	0.634	0.485–0.784	0.632	0.482–0.782	0.914
NS	0.545	0.392–0.699	0.518	0.363–0.672	0.204
NI	0.563	0.413–0.713	0.626	0.480–0.773	0.024
I	0.537	0.384–0.689	0.716	0.578–0.855	0.001
TI	0.613	0.461–0.765	0.705	0.561–0.849	0.002

AUC, area of under the receiver operating characteristic curve; PP-RNFL, peripapillary retinal nerve fiber layer thickness; PP Aver, average PP-RNFL; MT, macular thickness; MT Aver, average MT; GC-IPL, ganglion cell-inner plexiform layer thickness; GC-IPL Aver, average GC-IPL; S, superior; N, nasal; I, inferior; T, temporal; SN, superonasal; NS, nasosuperior; N, nasoinferior; IN, inferonasal; IT, inferotemporal; TI, temporoinferior; TS, temporosuperior; ST, superotemporal; Out S, outer superior; Out N, outer nasal; Out I, outer inferior; Out T, outer temporal; In S, inner superior; In N, inner nasal; In I, inner inferior; In T, inner temporal; TS, temporosuperior; NI, nasoinferior.
*Delong method was used for statistical analyses.

the DRI-OCT AUC in the inferior sector for the control versus moderate to severe glaucoma comparison (p=0.002) and in the nasoinferior, inferior, and temporoinferior sectors for the early glaucoma versus moderate to severe glaucoma comparison (p=0.024, p=0.001, and p=0.002, respectively).

DISCUSSION

In a previous study,[7] we assessed the repeatability and agreement of measurement results between DRI-OCT and Cirrus HD-OCT in normal eyes. According to the previous study, each OCT system showed different thickness values in the same measurement sector. PP-RNFL thickness obtained by DRI-OCT was larger than that obtained by Cirrus HD-OCT. However, GC-IPL thickness as measured by Cirrus HD-OCT was larger than that measured by DRI-OCT. These two OCT systems showed excellent repeatability in all measurement areas for normal subjects. Although the present study measured thickness for glaucoma patients, we expected that the repeatability of measurements for each OCT system would be maintained. In addition, as we discussed in the aforementioned study,[7] differences in thickness values between two OCT systems within same subjects might be attributed to differences in segmentation algorithm, measurement diameter, or light source. Even though there were differences between the thicknesses measured using the two OCT systems, their abilities to discriminate between normal and glaucomatous eyes using PP-RNFL, total macular, and GC-IPL thickness sector measurements were similar between two OCT devices in the present study. These results corroborate the results of recent studies showing similar abilities of DRI-OCT and spectral-domain-OCT to detect glaucomatous damage.[8-11] However, unlike a previous study,[8] we used 3D optic disc scanning of DRI-OCT for the measurement of PP-RNFL thickness. The wide scan mode of DRI-OCT, another scanning protocol used in previous studies, includes the area from the optic disc to the macula. Therefore, PP-RNFL thickness can be measured using the wide scan mode, and the measurements obtained are similar to those obtained using Cirrus HD-OCT optic disc scan.[8] However, they showed different thickness values from those obtained using the 3D optic disc scan in DRI-OCT.[9] In addition, regarding the shape of the scan area, 3D optic disc scan is more similar to the Cirrus HD-OCT than it is to the wide scan. Therefore, it is more reasonable to compare the PP-RNFL thicknesses obtained using the 3D optic disc scan in DRI-OCT and that in Cirrus HD-OCT. Another novel feature of our study was that we investigated sectoral PP-RNFL thickness not only in the 4 clock-hour sector but also in the 12 clock-hour sector. According to our data, average, superior, and inferior sectors of the peripapillary area showed high glaucoma diagnosis ability in both OCT modalities regardless of glaucoma severity. A thick RNFL bundle of vertical sectors explains the easier detection of RNFL change in the superior and inferior sectors.[15] This result is in line with those of previous studies that used time-domain OCT and/or spectral-domain OCT.[15-18] The macular area is another critical location for the diagnosis or follow-up of glaucoma because it is relatively free from confounding factors that can affect interpretation of the results, such as peripapillary atrophy, alignment of the measurement circle around the optic disc, and variable retinal vasculature.[19] The usefulness of full retinal thickness of the macular area for glaucoma detection has been shown in previous studies.[20-22] In addition, considering the importance of inner retinal layers in glaucomatous damage, it is thought that change in GC-IPL thickness is more related with glaucomatous damage.[15,23,24] In the present study, we could verify that both full macular thickness and GC-IPL thickness show good diagnostic ability for glaucoma. In particular, the high discriminative ability in the outer sectors for full macular thickness is consistent with the results obtained in previous studies.[22,25] Inner sectors of macular area are related with papillomacular fibers. Because these fibers get damaged later, the outer sectors are affected by glaucomatous change of the superior or inferior arcuate fibers in the early stage of glaucoma.

Our study results reflect the spatial distribution of nerve fibers. Hood, et al.[26-28] investigated the correspondence between functional and anatomical findings in the macula and peripapillary area using OCT and visual field test. They found that optic disc location affected how these corresponded.[27] Because the optic disc is located above the horizontal line that passes through the foveal center, inferior macular ganglion cells project to the inferotemporal and inferior optic disc margins. However, superior and nasal macular ganglion cells project to the temporal optic disc margin. This positional relationship was also identified in our study. Macular sectors with high discriminative abilities with both OCT systems were spatially well-matched with peripapillary sectors.

As in previous studies, discriminative ability was associated with glaucoma severity.[1,29,30] Among the three comparisons made in our study, the control versus moderate to severe glaucoma comparison had the largest AUC values in almost all peripapillary and macular measurement sectors examined. The control versus early glaucoma comparison tended to have higher AUC values than the early glaucoma versus moderate to severe glaucoma comparison, although this difference was not remarkable. Nouri-Mahdavi, et al.[30] investigated how well GC-IPL measurements can detect early glaucoma relative to RNFL measurements in the Cirrus HD-OCT. They showed that GC-IPL measurements have comparable glaucoma detection abilities to those found for PP-RNFL. Additionally, it was verified that inferior sectors within the PP-RNFL and GC-IPL measurement areas had the best glaucoma detection abilities. Our study also showed that inferior sector PP-RNFL and GC-IPL measurements are effective in distinguishing glaucomatous eyes from normal eyes. Interestingly, there were

https://doi.org/10.3349/ymj.2018.59.7.887

significant differences in inferior sectors for GC-IPL (inferior sector in control versus moderate to severe glaucoma and nasoinferior, inferior, and temporoinferior in early glaucoma versus moderate to severe glaucoma comparisons), where Cirrus HD-OCT AUC values were high. Further research is required to determine the clinical significance of our results. Our study had several limitations. A larger group of glaucomatous eyes would have allowed us to have more subgroups based on glaucoma severity. Additionally, prospective longitudinal studies should be conducted to examine how OCT systems can be used to detect glaucoma progression.

In conclusion, both OCT systems had similar abilities to discriminate between normal and glaucomatous eyes in critical thickness measurement sectors for glaucoma diagnosis for the adult Korean population, even though the 3D optic disc scan of DRI-OCT was used to measure PP-RNFL thickness. Together with the results of previous studies performed on other ethnic groups, our results verify the usefulness of DRI-OCT in diagnosis of glaucoma in comparison with Cirrus HD-OCT.

ACKNOWLEDGEMENTS

The authors are grateful to Hye Sun Lee (Department of Research Affairs, Biostatistics Collaboration Unit, Yonsei University College of Medicine, Seoul, Korea) for her help with the statistical analyses.

ORCID

Chan Yun Kim https://orcid.org/0000-0002-8373-9999

REFERENCES

1. Bussel II, Wollstein G, Schuman JS. OCT for glaucoma diagnosis, screening and detection of glaucoma progression. Br J Ophthalmol 2014;98 Suppl 2:ii15-9.
2. Leung CK. Diagnosing glaucoma progression with optical coherence tomography. Curr Opin Ophthalmol 2014;25:104-11.
3. Bae HW, Lee SY, Kim S, Park CK, Lee K, Kim CY, et al. Asymmetry of peak thicknesses between the superior and inferior retinal nerve fiber layers for early glaucoma detection: a simple screening method. Yonsei Med J 2018;59:135-40.
4. Gabriele ML, Wollstein G, Ishikawa H, Kagemann L, Xu J, Folio LS, et al. Optical coherence tomography: history, current status, and laboratory work. Invest Ophthalmol Vis Sci 2011;52:2425-36.
5. Mrejen S, Spaide RF. Optical coherence tomography: imaging of the choroid and beyond. Surv Ophthalmol 2013;58:387-429.
6. Lee SY, Kwon HJ, Bae HW, Seo SJ, Lee YH, Hong S, et al. Frequency, type and cause of artifacts in swept-source and cirrus HD optical coherence tomography in cases of glaucoma and suspected glaucoma. Curr Eye Res 2016;41:957-64.
7. Lee SY, Bae HW, Kwon HJ, Seong GJ, Kim CY. Repeatability and agreement of swept source and spectral domain optical coherence tomography evaluations of thickness sectors in normal eyes. J Glaucoma 2017;26:e46-53.
8. Yang Z, Tatham AJ, Weinreb RN, Medeiros FA, Liu T, Zangwill LM. Diagnostic ability of macular ganglion cell inner plexiform layer measurements in glaucoma using swept source and spectral domain optical coherence tomography. PLoS One 2015;10:e0125957.
9. Yang Z, Tatham AJ, Zangwill LM, Weinreb RN, Zhang C, Medeiros FA. Diagnostic ability of retinal nerve fiber layer imaging by swept-source optical coherence tomography in glaucoma. Am J Ophthalmol 2015;159:193-201.
10. Ha A, Lee SH, Lee EJ, Kim TW. Retinal nerve fiber layer thickness measurement comparison using spectral domain and swept source pptical coherence tomography. Korean J Ophthalmol 2016;30:140-7.
11. Lee KM, Lee EJ, Kim TW, Kim H. Comparison of the abilities of SD-OCT and SS-OCT in evaluating the thickness of the macular inner retinal layer for glaucoma diagnosis. PLoS One 2016;11:e0147964.
12. Chylack LT Jr, Wolfe JK, Singer DM, Leske MC, Bullimore MA, Bailey IL, et al. The lens opacities classification system III. The longitudinal study of cataract study group. Arch Ophthalmol 1993;111:831-6.
13. Budenz DL, Rhee P, Feuer WJ, McSoley J, Johnson CA, Anderson DR. Comparison of glaucomatous visual field defects using standard full threshold and Swedish interactive threshold algorithms. Arch Ophthalmol 2002;120:1136-41.
14. DeLong ER, DeLong DM, Clarke-Pearson DL. Comparing the areas under two or more correlated receiver operating characteristic curves: a nonparametric approach. Biometrics 1988;44:837-45.
15. Mwanza JC, Durbin MK, Budenz DL, Sayyad FE, Chang RT, Neelakantan A, et al. Glaucoma diagnostic accuracy of ganglion cell-inner plexiform layer thickness: comparison with nerve fiber layer and optic nerve head. Ophthalmology 2012;119:1151-8.
16. Medeiros FA, Zangwill LM, Bowd C, Vessani RM, Susanna R Jr, Weinreb RN. Evaluation of retinal nerve fiber layer, optic nerve head, and macular thickness measurements for glaucoma detection using optical coherence tomography. Am J Ophthalmol 2005;139:44-55.
17. Wollstein G, Schuman JS, Price LL, Aydin A, Stark PC, Hertzmark E, et al. Optical coherence tomography longitudinal evaluation of retinal nerve fiber layer thickness in glaucoma. Arch Ophthalmol 2005;123:464-70.
18. Mwanza JC, Oakley JD, Budenz DL, Anderson DR; Cirrus Optical Coherence Tomography Normative Database Study Group. Ability of cirrus HD-OCT optic nerve head parameters to discriminate normal from glaucomatous eyes. Ophthalmology 2011;118:241-8.e1.
19. Harwerth RS, Wheat JL, Fredette MJ, Anderson DR. Linking structure and function in glaucoma. Prog Retin Eye Res 2010;29:249-71.
20. Leung CK, Chan WM, Yung WH, Ng AC, Woo J, Tsang MK, et al. Comparison of macular and peripapillary measurements for the detection of glaucoma: an optical coherence tomography study. Ophthalmology 2005;112:391-400.
21. Ojima T, Tanabe T, Hangai M, Yu S, Morishita S, Yoshimura N. Measurement of retinal nerve fiber layer thickness and macular volume for glaucoma detection using optical coherence tomography. Jpn J Ophthalmol 2007;51:197-203.
22. Nakatani Y, Higashide T, Ohkubo S, Takeda H, Sugiyama K. Evaluation of macular thickness and peripapillary retinal nerve fiber layer thickness for detection of early glaucoma using spectral domain optical coherence tomography. J Glaucoma 2011;20:252-9.
23. Wang M, Hood DC, Cho JS, Ghadiali Q, De Moraes CG, Zhang X, et al. Measurement of local retinal ganglion cell layer thickness in patients with glaucoma using frequency-domain optical coherence tomography. Arch Ophthalmol 2009;127:875-81.
24. Lee JW, Morales E, Sharifipour F, Amini N, Yu F, Afifi AA, et al. The relationship between central visual field sensitivity and macular ganglion cell/inner plexiform layer thickness in glaucoma. Br J

Ophthalmol 2017;101:1052-8.
25. Nakano N, Hangai M, Nakanishi H, Mori S, Nukada M, Kotera Y, et al. Macular ganglion cell layer imaging in preperimetric glaucoma with speckle noise-reduced spectral domain optical coherence tomography. Ophthalmology 2011;118:2414-26.
26. Hood DC, Anderson SC, Wall M, Raza AS, Kardon RH. A test of a linear model of glaucomatous structure-function loss reveals sources of variability in retinal nerve fiber and visual field measurements. Invest Ophthalmol Vis Sci 2009;50:4254-66.
27. Hood DC, Raza AS, de Moraes CG, Liebmann JM, Ritch R. Glaucomatous damage of the macula. Prog Retin Eye Res 2013;32:1-21.
28. Hood DC, Wang DL, Raza AS, de Moraes CG, Liebmann JM, Ritch R. The locations of circumpapillary glaucomatous defects seen on frequency-domain OCT scans. Invest Ophthalmol Vis Sci 2013;54:7338-43.
29. Elbendary AM, Mohamed Helal R. Discriminating ability of spectral domain optical coherence tomography in different stages of glaucoma. Saudi J Ophthalmol 2013;27:19-24.
30. Nouri-Mahdavi K, Nowroozizadeh S, Nassiri N, Cirineo N, Knipping S, Giaconi J, et al. Macular ganglion cell/inner plexiform layer measurements by spectral domain optical coherence tomography for detection of early glaucoma and comparison to retinal nerve fiber layer measurements. Am J Ophthalmol 2013;156:1297-307.e2.

https://doi.org/10.3349/ymj.2018.59.7.887